

Survival of ultraheavy nuclei in astrophysical sources: applications to protomagnetar outflows

Nick Ekanger^{1,2,3,*}, Mukul Bhattacharya^{4,5,6}, Kohta Murase^{6,7}, and Shunsaku Horiuchi^{8,3,9}

¹*Frontier Research Institute for Interdisciplinary Sciences, Tohoku University, Sendai 980-8578, Japan*

²*Astronomical Institute, Graduate School of Science, Tohoku University, Sendai 980-8578, Japan*

³*Center for Neutrino Physics, Department of Physics, Virginia Tech, Blacksburg, VA 24061, USA*

⁴*Department of Physics, Wisconsin IceCube Particle Astrophysics Center,
University of Wisconsin, Madison, WI 53703, USA*

⁵*Department of Astronomy, Astrophysics and Space Engineering,
Indian Institute of Technology Indore, Simrol, MP 453552, India*

⁶*Department of Physics; Department of Astronomy & Astrophysics; Institute for Gravitation and the Cosmos,
The Pennsylvania State University, University Park, PA 16802, USA*

⁷*Center for Gravitational Physics and Quantum Information,
Yukawa Institute for Theoretical Physics, Kyoto University,
Kyoto, Kyoto 606-8502, Japan*

⁸*Department of Physics, Institute of Science Tokyo,
2-12-1 Ookayama, Meguro-ku, Tokyo 152-8551, Japan and*

⁹*Kavli IPMU (WPI), UTIAS, The University of Tokyo, Kashiwa, Chiba 277-8583, Japan*

(Dated: March 9, 2026)

Outflows of rapidly rotating protomagnetars have been considered as attractive sites for the synthesis of nuclei heavier than iron, but the question remains whether these nuclei are able to survive against photodisintegration as they make their way out of their formation environments. In this work, we present new analytic fitting formulae for the photodisintegration cross sections applicable to heavy nuclei beyond iron. We confirm that the results from the TALYS simulations are consistent with the theory of the giant dipole resonance, and apply the obtained new formulae to investigate whether ultraheavy nuclei entrained in protomagnetar outflows can be disintegrated by thermal and nonthermal photons before leaving the stellar envelope. We explore two outflow models: a spherical wind model and a jetted outflow model. For nuclei accelerated to the bulk speed of these outflows, their survival depends on the model and engine properties. For spherical winds, nuclei may survive for the first ~ 100 s post-core collapse, but as the wind Lorentz factor increases, the photodisintegration optical depth sharply rises and nuclei may no longer survive. For the jetted outflows arising from progenitors surrounded with stellar envelopes, nuclei can only survive before the jet breakout time in cases where the central engine has low spin-down energy, that is, with a low magnetic field strength and longer spin period. In progenitors with more extended envelopes, the jet break out time is much longer, allowing for nonthermal photons to readily photodisintegrate nuclei in high spin-down energy cases. These results also have implications for the capabilities of protomagnetars to source ultra-high energy cosmic ray nuclei.

I. INTRODUCTION

Ultrahigh energy cosmic rays (UHECRs), although observed for decades, are not fully understood (see Refs. [1–4] for reviews). Most recently, their flux and energy spectrum have been observed through the Pierre Auger Observatory (PAO; e.g., [5]) and Telescope Array (TA; e.g., [6]). The Greisen-Zatsepin-Kuzmin (GZK; [7, 8]) cutoff arises from the interaction of ultrahigh-energy protons with the cosmic microwave background (CMB), but the origin of the observed cutoff [9, 10] remains inconclusive.

While the sources of UHECRs still remain unknown, recent observations have provided important clues. For instance, at the highest energies, UHECRs are more likely to be of intermediate-to-heavy nuclei (see, e.g., [11]) and even ultraheavy nuclei may be present [12, 13], although the data cannot distinguish individual nuclei

that are present. Nevertheless, what has become clear is that the data disfavors the UHECR to be entirely composed of protons or protons and helium nuclei (see, e.g., [14, 15]). Understanding their composition will in turn facilitate a better understanding of the astrophysical sources that can produce UHECRs.

Proposed candidates of UHECR sources include jets from active galactic nuclei (AGNs, [16–20]), gamma-ray bursts including low-luminosity (LL) objects [21–25], newly born rapidly rotating magnetars arising from core-collapse supernovae (CCSNe, [26–29]), and binary neutron star mergers [13, 30–33]. An important requirement for any UHECR source is that the composition at the highest energies be enriched in nuclei relative to solar abundances [12]. In AGNs, such an enhancement may be achieved if jets reaccelerate pre-existing galactic cosmic rays, although this scenario can require tuning and remains uncertain [34–37]. For compact transients such as GRBs and engine-driven supernovae, as well as tidal disruption events (TDEs), it is natural that nuclei are supplied directly by their progenitor stars. If the progen-

* ekangernj@astr.tohoku.ac.jp

itor is rapidly rotating, the injected nuclear composition shaped by stellar evolution can reproduce the observed UHECR spectrum and composition [38–40] (see Ref. [41] for TDEs involving white dwarfs). Moreover, nuclei are not only inherited from stellar nucleosynthesis but can also be explosively synthesized during the first few seconds after core bounce. In this context, protomagnetar outflows are especially attractive because they can synthesize substantial abundances of intermediate-mass and heavy nuclei [42–46].

Such relativistic outflows launched by rapidly rotating, highly magnetized protoneutron stars (PNSs) formed in massive-star collapse are also a leading scenario for long-duration GRBs [47], making it plausible that the same engine both synthesizes heavy nuclei and accelerates them to ultrahigh energies. The resulting composition depends on the outflow properties (e.g., magnetization and time-dependent luminosity), which in turn follow from the spindown evolution of the central PNS (see [44]).

In addition to providing and accelerating nuclei, a viable UHECR source must allow them to survive, i.e., escape without disintegration [24, 48]. The main processes that can prevent heavy nuclei from escaping relativistic PNS outflows include photodisintegration, photomeson production, fragmentation, and nuclear spallation. Photodisintegration is particularly important because it shapes the maximum energy and the mass composition of nuclei during propagation through radiation fields [49–51]. These considerations generally favor low-luminosity jets and/or magnetically dominated outflows [24, 38–40, 42, 43, 48]. Low-power jets, including LL GRBs, may arise when relativistic jets are choked or partially smothered inside the progenitor envelope. The resulting phenomenology depends sensitively on the progenitor structure, e.g., Wolf–Rayet (WR) stars, blue supergiants (BSGs), and red supergiants (RSGs) (see Ref. [52] and references therein). Such events can exhibit properties intermediate between classical GRBs and transrelativistic supernovae [53], offering a unified picture of the GRB–SN connection, e.g., Refs. [54, 55].

Nuclei survival also affects multimessenger signatures: efficient photodisintegration can supply neutrons relevant for GeV neutrino production [56, 57], while stringent survival requirements can imply low ambient photon densities, thereby limiting high-energy neutrino production via photomeson interactions [58] or the escape of very high-energy gamma rays is guaranteed [24, 59, 60].

Motivated by this broader context, in this work we investigate whether nuclei synthesized via the r -process in protomagnetar-driven outflows can survive photodisintegration. Importantly, we focus on the fate of nuclei that are moving together with the bulk speed of the outflows, i.e., without assuming nonthermal components of ultra-heavy nuclei, including UHECRs.

The paper is organized as follows. In Sec. II, we examine photodisintegration cross sections in the dominant giant dipole resonance (GDR) channel and provide a new

approximation applicable to heavy nuclei with $A \geq 4$. In Sec. III, we introduce two protomagnetar outflow models and identify the timescales on which their photon fields transition from thermal to nonthermal. In Sec. IV, we compute the resulting photodisintegration optical depth and determine the conditions under which the nuclei can escape intact. We summarize the implications and discuss the remaining uncertainties in Sec. V and Sec. VI.

II. NEW FITTING FORMULAE OF PHOTODISINTEGRATION CROSS SECTIONS FOR HEAVY NUCLEI

To assess whether nuclei formed through explosive nucleosynthesis can avoid disintegration in environments with a significant number density of high-energy photons, we first describe how the photodisintegration cross sections depend on the nuclei mass number and energy. Here, we introduce an updated parametrization for the GDR cross section. GDR is the largest (in terms of cross section) and typically the most important resonance among photodisintegration processes, although there are additional photodisintegration processes that are relevant at higher energies.

We use the TALYS simulation tool (version 1.95, see [62, 63]) to calculate photodisintegration cross sections over the GDR and quasi-deuteron (QD) energy ranges (roughly $\sim 1 - 100$ MeV). Previous studies [24, 58] approximated the GDR cross section as $\sigma_{A\gamma} \approx \sigma_{\text{GDR}} \delta(\bar{\varepsilon} - \bar{\varepsilon}_{\text{GDR}}) \Delta\varepsilon_{\text{GDR}}$, where σ_{GDR} is the peak value of the GDR approximation, $\bar{\varepsilon}_{\text{GDR}} \sim 42.65A^{-0.21}$ MeV is the energy at which the resonance occurs and A is the nuclei mass number, and $\Delta\varepsilon_{\text{GDR}}$ is the resonance width. Previous studies like Ref. [61] (KT93) base this approximation on nuclear data up to iron ($Z = 26$, $A = 56$). To improve on this existing approximation by analyzing data from nuclei heavier than iron as well, we use TALYS to simulate the photonuclear cross sections for nuclei up to gold ($Z = 79$, $A = 197$). We use this TALYS data to then determine the approximate height of the GDR resonance (σ_{GDR}), peak energy for resonance ($\bar{\varepsilon}_{\text{GDR}}$), and its width ($\Delta\varepsilon_{\text{GDR}}$), where this width is defined as the full width at half maximum of the peak. This is a valid approximation since the majority of the GDR cross section outputs given by TALYS are roughly symmetric-Lorentzian functions.

We find that $\bar{\varepsilon}_{\text{GDR}} \approx 42.65A^{-0.21}$ MeV fits the TALYS data for the central energy of the GDR resonance well, as shown in the *top right panel* of Fig. 1. In the same figure, we also show new fits to σ_{GDR} (in the *top left panel*), $\Delta\varepsilon_{\text{GDR}}$ (in the *bottom left panel*), and the product of the two since this is proportional to $\sigma_{A\gamma}$ (in the *bottom right panel*). From the variation of σ_{GDR} with mass number A , we find that σ_{GDR} scales with an approximately linear dependence on the mass number up to iron ($A = 56$). However, a power law with $\sigma_{\text{GDR}} \propto A^{4/3}$ is a better fit for larger mass numbers up to $A \sim 200$. For example, in Ref. [24], a constant $\Delta\varepsilon_{\text{GDR}} \approx 8$ MeV is assumed, but

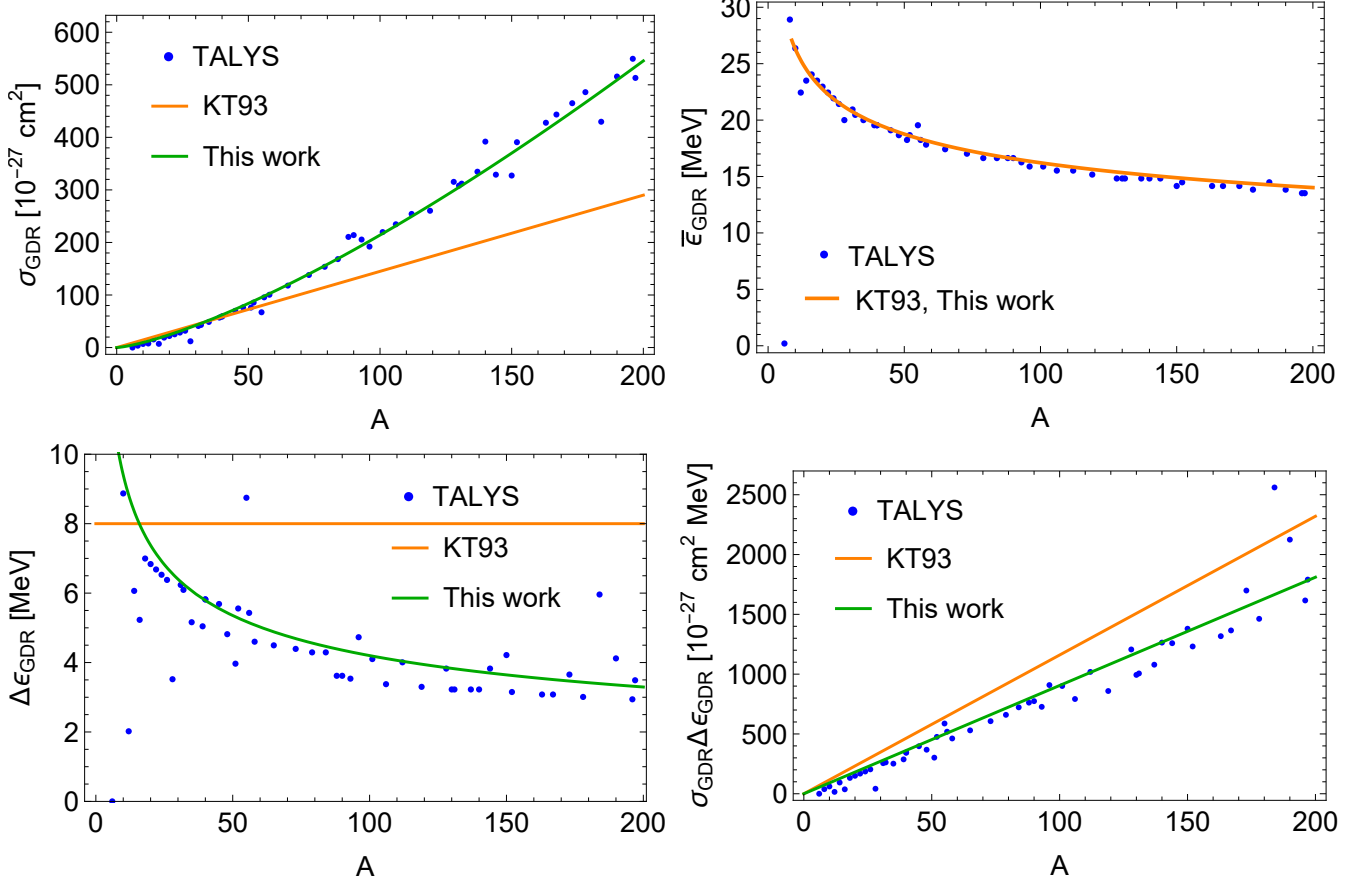


FIG. 1. The TALYS data (shown as blue dots in each panel) compared to old fits (orange lines, see [61] (henceforth KT93)) and our new fits (green lines in each panel, except for the *top right* panel where our fit is the same as KT93). *Top left*: the TALYS peak cross-section data (σ_{GDR} , see Eq. (1)) for GDR resonance. The best fit can be described by a power law $\sigma_{\text{GDR}} \approx 0.43A^{1.35} \times 10^{-27} \text{ cm}^2$. *Top right*: the best fit to TALYS data for the central energy ($\bar{\epsilon}_{\text{GDR}}$) of the GDR resonance, in which case the prior fit describes the data well. The best fit is given by $\bar{\epsilon}_{\text{GDR}} \approx 42.65A^{-0.21} \text{ MeV}$. *Bottom left*: the full-width at half-maximum ($\Delta\epsilon_{\text{GDR}}$) of the TALYS data versus A . The best fit is given by $\Delta\epsilon_{\text{GDR}} \approx 21.05A^{-0.35} \text{ MeV}$, in contrast to a constant value of 8 MeV used in the previous studies. *Bottom right*: the product $\sigma_{\text{GDR}}\Delta\epsilon_{\text{GDR}} \approx 9A \times 10^{-27} \text{ cm}^2 \text{ MeV} \propto \sigma_{A\gamma}$, resulting in an approximately linear A -dependence.

here we update this to a different power law given by $\approx 21.05A^{-1/3} \text{ MeV}$.

The best-fit parametrizations are as follows: $\sigma_{\text{GDR}} \approx 0.43 \times 10^{-27} A^{1.35} \text{ cm}^2$, $\bar{\epsilon}_{\text{GDR}} \approx 42.65A^{-0.21} \text{ MeV}$, $\Delta\epsilon_{\text{GDR}} \approx 21.05A^{-0.35} \text{ MeV}$, such that the GDR cross section scales linearly with mass number,

$$\begin{aligned} \sigma_{A\gamma} &\approx \sigma_{\text{GDR}}\Delta\epsilon_{\text{GDR}}\delta(\bar{\epsilon} - \bar{\epsilon}_{\text{GDR}}) \\ &\approx (0.43A^{1.35} \times 10^{-27} \text{ cm}^2)\delta(\bar{\epsilon} - 42.65A^{-0.21} \text{ MeV}) \\ &\quad \times (21.05A^{-0.35} \text{ MeV}). \end{aligned} \quad (1)$$

These results are also listed in Table I, where we compare our results with previous approximations. Note that in our results, the total cross section is linear with mass number A , but the prefactor and width have different A dependencies. Ref. [64] finds $\sigma_{\text{GDR}} \sim 0.48A^{4/3} \times 10^{-27} \text{ cm}^2$ which is very similar to the value of $0.43A^{1.35} \times 10^{-27} \text{ cm}^2$ obtained in this work, although different values of $\bar{\epsilon}_{\text{GDR}}$ and $\Delta\epsilon_{\text{GDR}}$ are inferred.

In the Goldhaber-Teller picture [65], GDR is the dominant isovector collective mode in which the proton and neutron fluids oscillate out of phase as two slightly displaced liquid drops, producing a large electric dipole (E1) moment. It is known that the E1 strength is largely concentrated in this collective resonance. The contribution from the GDR region to the energy-weighted E1 sum is a large fraction of the total Thomas-Reiche-Kuhn (TRK) sum rule. Since the TRK sum scales as NZ/A , where N is the number of neutrons, the integrated photodisintegration cross section is $\int \sigma_{A\gamma} d\bar{\epsilon} \propto NZ/A$. For heavy nuclei, this gives $NZ/A \sim A/4$ and hence $\int \sigma_{A\gamma} d\bar{\epsilon} \approx \sigma_{\text{GDR}}\Delta\bar{\epsilon}_{\text{GDR}} \propto A$. If the relevant restoring force is governed mainly by bulk nuclear properties, the corresponding frequency is $\Gamma \propto R^{-1} \propto A^{-1/3}$, leading to $\bar{\epsilon}_{\text{GDR}} \propto A^{-1/3}$. If the dominant damping is controlled by surface-related decoherence, one expects $\Delta\bar{\epsilon}_{\text{GDR}} = \Gamma \sim \hbar/\tau \propto R^{-1} \propto A^{-1/3}$, and therefore $\sigma_{\text{GDR}} \propto A^{4/3}$ is expected.

	σ_x	Prefactor [10^{-27} cm^2]	Center [MeV]	Width [MeV]	A-range
<i>This work</i>	σ_{GDR}	$0.43A^{1.35}$	$42.65A^{-0.21}$	$21.05A^{-0.35}$	$4 \leq A \leq 197$
<i>Karakula and Tkaczyk [61]</i>	σ_{GDR}	$1.45A$	$42.65A^{-0.21}$	8.0	$56 > A > 4$
	σ_{GDR}	$1.45A$	$0.925A^{-2.433}$	8.0	$A \leq 4$

TABLE I. Comparison of cross section approximations relevant in this work for the disintegration of nuclei. Here, the GDR approximation is of the form $\sigma_x \approx (\text{Prefactor})\delta(\bar{\varepsilon} - \text{Center})(\text{Width})$. A -range describes the range of mass numbers for which the approximation is valid.

Although the best-fit approximation for σ_{GDR} and $\Delta\varepsilon_{\text{GDR}}$ agree well with the TALYS data points, there are some notable outliers - especially in the case of $\Delta\varepsilon_{\text{GDR}}$ for smaller mass numbers. Some nuclei have cross sections that are not well described by Lorentzian functions and/or have double peaks, such as carbon-14, oxygen-16, silicon-28, vanadium-51, and manganese-55. Most nuclei, however, are well described by a single Lorentzian function.

We do not consider higher-energy photodisintegration resonances, photomeson production and fragmentation, because GDR is the predominant photonuclear interaction in the photon energy range of interest. Further, TALYS does not simulate resonances beyond the pion production threshold. Tools like the Geant4 toolkit [66] and other analytical formulae can model these processes, but are not considered here (see [24, 67, 68] for the impacts of higher-energy photodisintegration processes). Spallation is another process that can lead to the destruction of nuclei and may have a minor impact on the results of nucleus survival for some scenarios (see Sec. V for discussion on this point).

III. APPLICATIONS TO PROTONEUTRON STAR OUTFLOWS

The cross section formulae we provide can be used for many astrophysical sources. In this section, we explore two models of protomagnetar-driven outflows: the spherical wind and jetted outflow models. Figure 2 shows the schematic picture of these two models. Below, we determine the evolution of the (non)thermal nature of the photon spectra. Then, in Sec. IV, we will discuss the time evolution of the photodisintegration optical depth.

A. Photon analysis framework

Within the wind, nuclei are exposed to high-energy photons which may disintegrate them into nucleons. In order to determine whether the nuclei get destroyed, we first determine the energy distribution of these photon fields. To do this, we calculate the Thomson optical depth, τ_T , to determine whether photons are thermalized due to copious electron-positron pairs in the wind.

This is given by

$$\tau_T \approx y_{\pm} n_x \sigma_T R_x / \Gamma_x, \quad (2)$$

where the subscript ‘x’ describes either the spherical wind (w) or jetted outflow (h) model (see subsections below). Additionally, $y_{\pm} = (n_x + n_{\pm})/n_x$ is the pair production enhancement factor where $n_x = \dot{M}_x / (4\pi R_x^2 m_p c \Gamma_x)$ is the wind baryon number density and $n_{\pm} = \dot{M}_{\pm} / (4\pi R_x^2 m_e c \Gamma_x)$ is the pair number density, Γ_x is the Lorentz factor of the outflow, $\dot{M}_{\pm} \approx (2.5 \times 10^{-17} M_{\odot} \text{ s}^{-1}) \mu_{\pm,6} B_{\text{dip},15} P_{i,-2}^{-2} R_{\text{NS},6}^3$ is the Goldreich-Julian (GJ) mass-loss rate [69]. Here, $\mu_{\pm} \approx 10^6$ is the pair multiplicity [70, 71], B_{dip} is the dipole magnetic field strength and P_i is the spin period of the PNS. The Thomson cross section is given by $\sigma_T = 6.65 \times 10^{-25} \text{ cm}^2$. In this study, we consider outflows with $10^{13} \text{ G} < B_{\text{dip}} < 10^{15} \text{ G}$ and $1 \text{ ms} < P_i < 30 \text{ ms}$.

The distribution of the photon spectrum will have quantitative impacts on nuclear survivability. To help understand the evolution of the photon spectrum, we label the approximate time when photons transition when the system is optically thin as t_{Th} ; this timescale is defined as the time when $\tau_T = 1$. This should be understood as a proxy because the details depend on radiative transfer calculations. Nevertheless, it will suffice for the outflow models we consider. In the following sections, we explore a spherical wind model and a jetted outflow model that are driven by rapidly rotating, high magnetized protoneutron stars. Whether particles can remain as undestroyed nuclei and escape the system depends, then, on: (A) the timescale after which the outflow transitions from thermal to nonthermal photon-dominated system (t_{Th}), and (B) the timescale at which the nuclei are transported outside the progenitor.

B. Spherical wind

The schematic picture of the spherical wind is shown in the *left panel* of Fig. 2 with two regions: the neutrino-driven wind (Region A) and the shocked pulsar wind nebula (PWN, Region B). In this picture, the relativistic wind (A) catches up to the nonrelativistic PWN (B) over time. In this section, we describe how we calculate τ_T (Eq. 2) in both these regions.

In Region A, we calculate the wind radius R_w and ejecta radius R_{ej} by numerically solving the differential

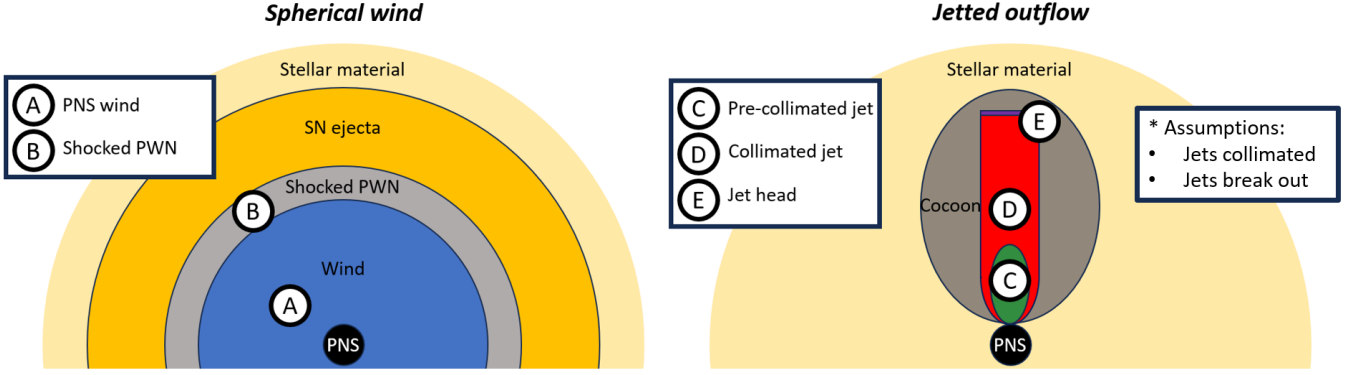


FIG. 2. Schematic picture of the two models we consider. *Left panel*: a spherical wind originating from the protomagnetar central engine. In Region A, a neutrino-driven wind flows from the PNS central engine, which eventually catches up to the nonrelativistic pulsar wind nebula in Region B. *Right panel*: a jetted outflow which may also originate from protomagnetar central engines. In Region C, a pre-collimated jet expands into Region D, which is a collimated jet region. Region E is the jet head, which may break out of the surrounding stellar material.

equations [72, 73],

$$\frac{dR_w}{dt} = \sqrt{\frac{7}{6(3-\delta)} \frac{\mathcal{E}_{\text{tot}}}{M_{\text{ej}}} \left(\frac{R_w}{R_{\text{ej}}}\right)^{3-\delta}} + \frac{R_w}{t} \quad (3)$$

$$\frac{dR_{\text{ej}}}{dt} \equiv V_{\text{ej}} = \sqrt{\frac{2\mathcal{E}_{\text{tot}}}{M_{\text{ej}}}}, \quad (4)$$

where $\delta = 1$ is used for the density profile of the ejecta. We assume an ejecta mass of $M_{\text{ej}} = 3M_{\odot}$ and SN explosion energy of $\mathcal{E}_{\text{tot}} = 10^{51}$ erg. We set $R_w(t=0) = R_{\text{ej}}(t=0) = R_{\text{LC}} = cP_i/2\pi$ as the initial conditions, where R_{LC} is the radius of the light cylinder.

The mass-loss rate from the PNS surface due to the wind driven by neutrinos is given by [74],

$$\dot{M}_w = (5 \times 10^{-5} M_{\odot} \text{ s}^{-1}) \left[\frac{L_{\nu}}{10^{52} \text{ erg s}^{-1}} \left(\frac{\varepsilon_{\nu}}{10 \text{ MeV}} \right)^2 \right]^{5/3} \times \mathcal{F}_{\text{mag}} \left(C_{\text{inel}} \frac{R_{\text{NS}}}{10^6 \text{ cm}} \right)^{5/3} \left(\frac{M_{\text{NS}}}{1.4 M_{\odot}} \right)^{-2}. \quad (5)$$

Several correction factors are accounted for here, including $\mathcal{F}_{\text{mag}} = f_{\text{op}} f_{\text{cen}}$ which considers the fraction of the PNS surface threaded by open magnetic field lines (f_{op}) and an enhanced mass loss rate due to magnetorotational slinging (f_{cen}), C_{inel} for inelastic neutrino-electron scatterings, and a stretch factor of $\eta_s = 3$ to model longer PNS cooling timescales due to rapid rotation (for these, see Ref. [74]). L_{ν} is the $\nu_e + \bar{\nu}_e$ neutrino luminosity, ε_{ν} is the mean neutrino energy, R_{NS} is the PNS radius, and M_{NS} is the PNS mass. We choose $M_{\text{NS}} = 1.4 M_{\odot}$ and $R_{\text{NS}} = 10^6$ cm based on Ref. [75]. The PNS mass outflow rate eventually transitions from being baryon-dominated to pair-dominated. This occurs when $\dot{M}_x = \dot{M}_{\pm}$ is attained (hereafter, labeled with $t = t_{\text{GJ}}$). Thus, if $t_{\text{Th}} > t_{\text{GJ}}$, the nuclei are likely to face thermal photons, while if $t_{\text{Th}} < t_{\text{GJ}}$, nuclei can also encounter nonthermal photons.

The Lorentz factor of the wind, $\Gamma(r = R_w) = \Gamma_w$, can be expressed as [76],

$$\Gamma = \begin{cases} \sigma_0 (r/R_{\text{mag}})^{1/3}, & r \leq R_{\text{mag}} \\ \sigma_0, & r > R_{\text{mag}} \end{cases}, \quad (6)$$

where r is evaluated at R_w and R_{mag} is the magnetic dissipation radius given by $R_{\text{mag}} \approx (5 \times 10^{12} \text{ cm})(\sigma_0/10^2)^2 (P/\text{ms})(\varepsilon/0.01)^{-1}$. We parametrize the reconnection velocity with $\varepsilon \sim 0.01$ [74]. Wind magnetization is $\sigma_0 = \phi_B^2 \Omega^2 / \dot{M}_w c^3$, where $\phi_B = (f_{\text{op}}/4\pi) B_{\text{dip}} R_{\text{NS}}^2$ is the magnetic flux from a rotating dipole field (of strength B_{dip}) and Ω is the PNS angular velocity.

In Region B, we also calculate the Thomson optical depth at $R_x = R_w$, assuming $\dot{M}_x = \dot{M}_w$, but because the outflow is nonrelativistic, $\Gamma_x = 1$ and $n_x = \dot{M}_w / (4\pi R_w^2 m_p V_w)$ where $V_w = dR_w/dt$.

The *left panel* of Fig. 3 shows τ_T as a function of time post core-collapse for the spherical wind model in the shaded blue region (Region A) and in the shaded gray region (Region B). The width of this shaded region reflects the values for the B_{dip} and P_i configurations used in this work, where the edges stand for the minimum and maximum values of τ_T . The horizontal dashed black line denotes $\tau_T = 1$ when the photon distribution transitions from thermal to nonthermal, which generally occurs around 100–300 s. Finally, the shaded gray region shows the range in times $t = t_{\text{GJ}} \sim 300 - 500$ s, corresponding to the range in B_{dip} and P_i , at which the outflow mass becomes dominated by electron-positron pairs instead of baryons. For all spherical wind models, we find $t_{\text{Th}} < t_{\text{GJ}}$, such that nuclei in the outflow can encounter nonthermal photons before the mass outflow rate drops considerably to be pair dominated.

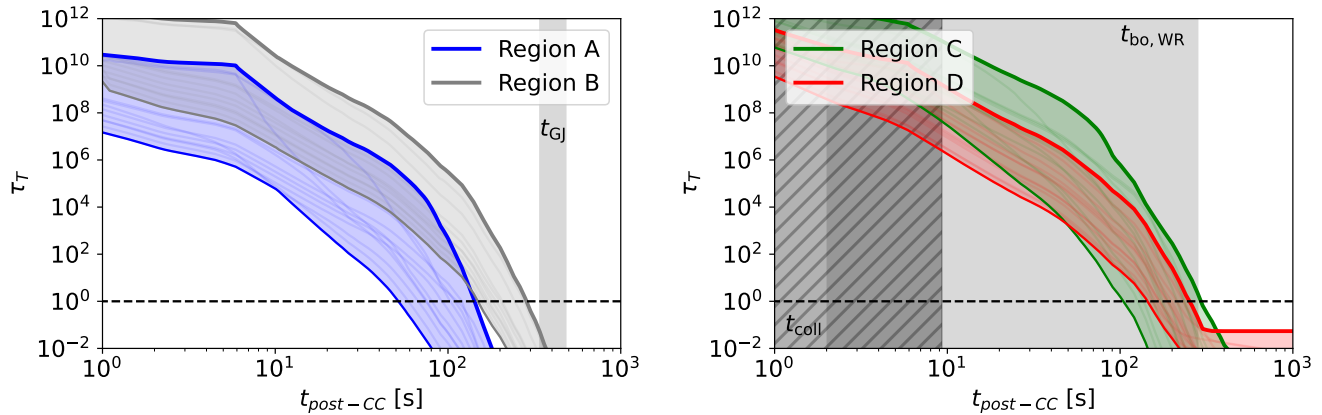


FIG. 3. Thomson optical depth, τ_T , for several cases is shown as a function of time. The dashed black line shows $\tau_T = 1$. The shaded regions represent the minimum to maximum τ_T values that are calculated for our range of B_{dip} and P_i configurations and the translucent lines between are the individual results for each configuration. The gray hatched region represents the time when the jets become collimated (t_{coll}) and the gray shaded region is the breakout time for WRs ($t_{\text{bo,WR}}$). For all cases, $t_{\text{coll}} < t_{\text{bo}}$. *Left panel:* τ_T , for the spherical wind case for Regions A (blue shaded) and B (gray shaded). The vertical gray shaded region shows the range in t_{GJ} values for our range of B_{dip} and P_i configurations. For all configurations of B_{dip} and P_i , $t_{\text{Th}} < t_{\text{GJ}}$, implying that nonthermal photons are expected by t_{GJ} . *Right panel:* τ_T for the jetted outflow case of a WR progenitor in Regions C (green shaded) and D (red shaded). After $t_{\text{bo,WR}}$, nuclei can freely escape the star. For WRs, $t_{\text{Th}} > t_{\text{bo,WR}}$ (except for one case), for BSGs, $t_{\text{Th}} > t_{\text{bo,BSG}}$ for rapidly rotating engines, and for all RSG cases, $t_{\text{Th}} < t_{\text{bo,RSG}}$.

C. Jetted outflow

If the outflow propagates through dense stellar material, it may become collimated. A cocoon forms as the outflow interacts with the surrounding medium and the subsequent magnetized outflow can burrow through the star like a jet. Such different outflow geometries can lead to different distributions of photons. Such a scenario is shown in the *right panel* of Fig. 2. Here, region C is the pre-collimated jet outflow, Region D is the collimated jet, and Region E is the jet head. In this work, we do not consider the survival of nuclei in the cocoon region or the jet head, but only in the pre-collimated and collimated jets. Typically, the cocoon's energy density is low enough for nuclei survival [43]. Because the outflows are jetted, the number density of the baryons is increased by a factor of $(\theta_j^2/2)^{-1}$ [52]. We choose a jet with a fixed opening angle of $\theta_j = 10^\circ$ at the jet launch site near the PNS.

In Region C, $R_x = R_{\text{cs}}$, or the radius of the collimation shock (see Sec. 3.3 in Ref. [52]), $\Gamma_x = \Gamma_j = \Gamma(r = R_{\text{cs}})$, and $n_x = \dot{M}_w / (4\pi R_{\text{cs}}^2 m_p c \Gamma_j) / (\theta_j^2/2)$. In the collimated jet of Region D, $R_x = \min(R_*, R_h) = R_h$ (until the jet break outs of the progenitor), $\Gamma_x = \Gamma_{\text{cj}} = 1/\theta_j$, and $n_x = \dot{M}_w / (4\pi R_h^2 m_p c \Gamma_{\text{cj}}) / (\theta_j^2/2)$. The cocoon that forms can be approximately modeled as a cylinder, whose head radius is described as $R_h = c\xi_h\beta_h t$, where $\xi_h = (5 - \alpha)/3$ is a coefficient, $\alpha \sim 2 - 3$ is the power-law index of the density profile, and β_h is the velocity of the jet head (see [52], Eq. (7)). As the figure shows, we have implicitly assumed collimation. While jets begin as uncollimated, we find that all become collimated (when $R_h > R_{\text{cs}}$) quickly within $t_{\text{coll}} < 10$ s. The exact tim-

ing depends on both outflow properties as well as the stellar progenitor. For the former, we consider outflows with $10^{13} \text{ G} < B_{\text{dip}} < 10^{15} \text{ G}$ and $1 \text{ ms} < P_i < 30 \text{ ms}$. For the latter, we consider a smaller/denser WR star and an extended/sparser blue and red supergiants (BSG, RSG).

We estimate the jet breakout time, t_{bo} , for WR progenitors using the analytical expression from the text after Eq. (1) in [44] (see also, Eq. (12) in [45]). This expression takes into account the $B_{\text{dip}} - P_i$ configuration and signifies when the magnetized outflow has met the minimum energy requirement necessary to break out of the stellar surface (see also [77]). Our WR, BSG, and RSG progenitor stars have radii of $R_* = 5.15 R_\odot$, $52 R_\odot$, and $875 R_\odot$, respectively (see [52], for the details of their density profiles and how they lead to different jet structures). As a simple estimate, we calculate the breakout times for BSGs and RSGs using the ratio of their radii to WR radii, i.e., $t_{\text{bo,BSG}} \sim 10 \times t_{\text{bo,WR}}$ and $\sim 170 \times t_{\text{bo,WR}}$, because the velocity of the jet head does not change significantly over time. In this study, we do not consider choked jets that do not breakout of their WR progenitors; these jets may arise from central engines that do not have sufficient isotropic jet luminosity to break out ($B_{\text{dip}} \lesssim 3 \times 10^{15} \text{ G}$, roughly independent of P_i) [52].

The jet breakout time has an impact on the window over which the nuclei are exposed to energetic photons within the jet. If $t_{\text{Th}} > t_{\text{bo}}$, the photons are thermalized even after breakout. Since the jet breaks out of the star before the surrounding photons become nonthermal, the nuclei only interact with lower energy thermal photons. On the other hand, if $t_{\text{Th}} < t_{\text{bo}}$, the photons can contain a nonthermal component before breakout. Timescales,

as in the spherical wind case, are dependent on B_{dip} and P_i , but also have a strong dependence on the progenitor's stellar radius.

Figure 3 (*right panel*) shows τ_T as a function of time post core-collapse for the jetted outflow models of WR progenitors. In green we show the range of optical depth values for Region C, and in red we show the range of values for Region D. The dark gray hatched region at early times is the time over which the jets become collimated and, in this region, our calculations are not valid. The gray shaded region shows the range of breakout times $t_{\text{bo,WR}}$ for various $B_{\text{dip}} - P_i$ configurations. To check the validity of our calculations up to breakout time, we confirm that $t_{\text{coll}} < t_{\text{bo}}$ for all jets.

For all outflows in WRs (except the $B_{\text{dip}} = 10^{13}$ G, $P_i = 30$ ms case), $t_{\text{Th}} > t_{\text{bo,WR}}$. This suggests that nuclei only encounter thermal photons before breaking out and escaping the stellar envelope. For BSGs, $t_{\text{Th}} > t_{\text{bo,BSG}}$ for the rapidly rotating cases we consider. Thus, nuclei in the slowly rotating progenitors encounter non-thermal photons before the jet breaks out. For RSGs, $t_{\text{Th}} < t_{\text{bo,RSG}}$ for all cases, and the photons can be non-thermal in all jets that we consider. Further, $t_{\text{Th}} < t_{\text{GJ}}$, where $t_{\text{GJ}} \sim 300 - 500$ s as in the *left panel* of Fig. 3. The high B_{dip} configurations tend to transition to nonthermal photons earlier, primarily due to a lower number density. Thus, progenitors with smaller envelopes do not typically undergo the transition from thermal to nonthermal photons prior to breakout. The survival consequences because of this are explored in Sec. IV.

IV. EFFECTIVE PHOTODISINTEGRATION OPTICAL DEPTH

In Sec. III, we evaluated the timescale (t_{Th}) at which different outflow models transition from a thermal photon field to potentially hosting also a nonthermal photon field and the time at which the nuclei may escape their environment. In this section, we investigate nucleus survival and the extent to which this depends on the photon distribution. To do this, we calculate the photodisintegration optical depth as a function of time.

The effective photodisintegration optical depth is estimated as

$$f_{A\gamma} = t_{A\gamma}^{-1} t_{\text{dyn}}, \quad (7)$$

where $t_{\text{dyn}} = R_x/(\Gamma_x c)$ is the dynamical timescale of the outflow and the photodisintegration timescale is (e.g., Ref. [24])

$$t_{A\gamma}^{-1} = \frac{c}{2\gamma_A^2} \int_{\bar{\varepsilon}_{\text{th}}}^{\infty} d\bar{\varepsilon} \sigma_{A\gamma}(\bar{\varepsilon}) \kappa_{A\gamma}(\bar{\varepsilon}) \bar{\varepsilon} \int_{\bar{\varepsilon}/2\gamma_A}^{\infty} d\varepsilon \varepsilon^{-2} \frac{dn}{d\varepsilon}. \quad (8)$$

Here, $\gamma_A = E_A/m_A c^2$ is the nucleus Lorentz factor, $\bar{\varepsilon}_{\text{th}} \sim 10$ MeV is the photodisintegration threshold energy, $\sigma_{A\gamma}$ is the photodisintegration cross section, $\kappa_{A\gamma} \sim 1/A$ is the nucleus inelasticity, $dn/d\varepsilon$ is the photon energy spectrum

that the nuclei are exposed to, ε is the photon energy in the comoving frame and $\bar{\varepsilon}$ denotes the photon energy in the nucleus rest frame. In this work, we assume that nuclei are accelerated to the bulk Lorentz factor of each region, i.e., $E_A = \Gamma_x m_A c^2$.

Prior to $t = t_{\text{Th}}$, τ_T is much larger than unity, resulting in a thermal photon distribution described by,

$$\frac{dn}{d\varepsilon} = \frac{8\pi}{(hc)^3} \frac{\varepsilon^2}{e^{\varepsilon/k_B T_\gamma} - 1}, \quad (9)$$

where T_γ is the photon temperature, related to the gamma-ray energy density by $U_\gamma = aT_\gamma^4$. This distribution results in an analytical expression for $f_{A\gamma}$,

$$f_{A\gamma} = \frac{4\pi c \sigma_{\text{GDR}} \Delta \varepsilon_{\text{GDR}} \bar{\varepsilon}_{\text{GDR}}}{A \gamma_A^2 (hc)^3} k_B T \ln(1 - e^{-y})^{-1} t_{\text{dyn}}, \quad (10)$$

where $y = \bar{\varepsilon}_{\text{GDR}}/(2\gamma_A k_B T)$. We suggest that nuclei undergo significant disintegration when $f_{A\gamma} \gtrsim 1$.

After t_{Th} , $\tau_T < 1$ and we describe the nonthermal distribution with a broken power law:

$$\frac{dn}{d\varepsilon} = \mathcal{N} \frac{(1 - e^{-\tau_{\gamma\gamma}})}{\tau_{\gamma\gamma}} \begin{cases} (\varepsilon/\varepsilon_{\text{break}})^{-\alpha}, & \varepsilon_{\text{min}} < \varepsilon < \varepsilon_{\text{break}} \\ (\varepsilon/\varepsilon_{\text{break}})^{-\beta}, & \varepsilon_{\text{break}} \leq \varepsilon \end{cases} \quad (11)$$

where \mathcal{N} is the normalization, $\varepsilon_{\text{min}} \sim \varepsilon_{\text{ssa}} \sim 1$ eV is the minimum photon energy allowed by synchrotron self-absorption [24], $\varepsilon_{\text{break}}$ is the break energy, and $\tau_{\gamma\gamma}$ is the optical depth of e^+e^- pairs created through photon annihilation [78]. We choose $\varepsilon_{\text{break}} = 10^{2.5}$ keV in the comoving frame and the low/high photon spectra indices of $\alpha = 1$ and $\beta = 2.2$ [24]. The normalization of the photon spectrum, \mathcal{N} , is chosen such that the radiation energy density, $U_\gamma = \int \varepsilon dn/d\varepsilon d\varepsilon$, is always conserved. To finally calculate the photodisintegration optical depth, we need to define the energy density of the photons and dynamical timescale in each region.

A. Spherical wind

In Region A, the energy density is related to the baryonic mass-loss of the neutrino-driven wind: $U_{\gamma,A} = \epsilon_\gamma \Gamma_w (M_w + M_\pm) c^2 / (4\pi \Gamma_w^2 R_w^2 c)$, where $\epsilon_\gamma = 0.3$ is the fraction of the energy converted to radiation. The dynamical timescale is given by $t_{\text{exp,A}} = R_w / (\Gamma_w c)$. In Region B, however, the energy density is proportional to the spin-down luminosity of the proton-neutron star engine: $U_{\gamma,B} = \epsilon_e L_{\text{spin}} / (4\pi R_w^2 c)$, where $\epsilon_e \sim 1$ is the fraction of energy converted to electrons and positrons, and L_{spin} is the electromagnetic spin-down luminosity (or equation 5) of Ref. [72]. The dynamical timescale is given by $t_{\text{exp,B}} = R_w / V_w$. Finally, photons leak from Region B into Region A, with an energy density of $U_{\gamma,BA} = f_{\text{BA}} U_{\gamma,B} \Gamma_w^2$, where $f_{\text{BA}} = \min(1/\tau_{T,B}, 1)$ is the leakage fraction.

In Fig. 4, we show $f_{A\gamma}$ as a function of time post-core collapse for our two physical model scenarios. In each

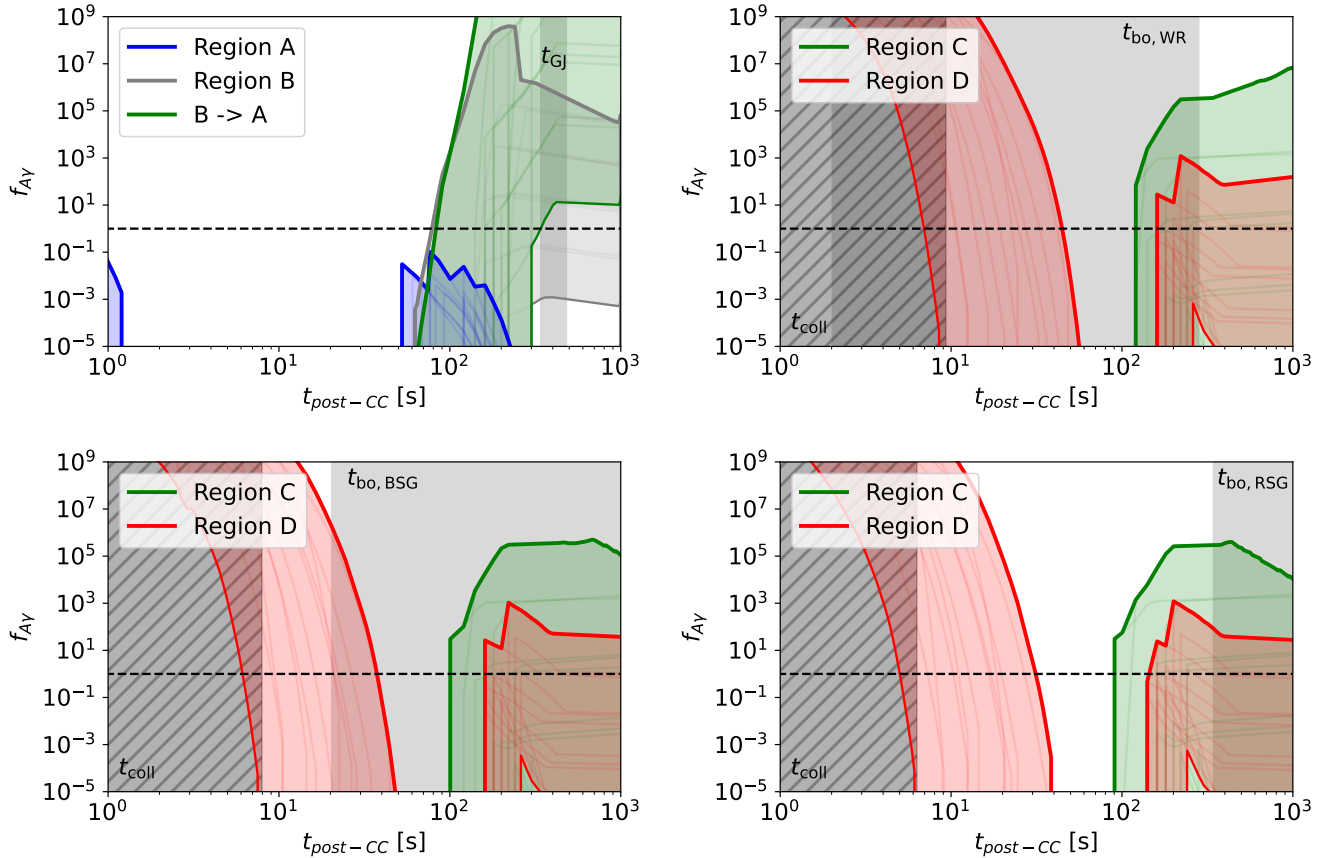


FIG. 4. The photodisintegration optical depth, $f_{A\gamma}$, is shown as a function of time post core-collapse. In each panel, the value of $f_{A\gamma} = 1$ is denoted by the horizontal dashed black line assuming a pure-iron composition ($A = 56$). The nuclei energy is assumed to be $\Gamma_x m_A c^2$, where Γ_x is the bulk Lorentz factor in each Region. The shaded colored regions show the extent of values when varying the PNS magnetic field and spin period, whose boundaries are given by the maxima and minima values found. The lines within these regions correspond to the individual B_{dip}/P_i configurations. The hatched t_{coll} region shows the time when the jets become collimated, before which the calculations are unphysical. Finally, the shaded gray regions show the extent of breakout times for each case. *Top left panel:* $f_{A\gamma}$ for the spherical wind case. For the first ~ 100 s (t_{Th} for Region A), $f_{A\gamma} \ll 1$ so nuclei can survive in both regions. Around this time, photons become nonthermal, but the energy density is not high enough in Region A to cause photodisintegration. However, very quickly, due to leaked photons in Region A and Region B, nuclei are efficiently destroyed. *Top right panel:* $f_{A\gamma}$ for the jetted outflow case from WR progenitors. In some high P_i cases, $f_{A\gamma} \gg 1$ in the regime where thermal photons can destroy nuclei before the breakout time. In all other cases, nuclei can survive photodisintegration before breaking out of the star. *Bottom left panel:* $f_{A\gamma}$ for the jetted outflow case from BSG progenitors. In this scenario, $f_{A\gamma} < 1$ for all cases at $t_{\text{bo,BSG}}$ (except the case of $B_{\text{dip}} = 10^{15}$ G, $P_i = 10$ ms, where $f_{A\gamma} \sim 1$). *Bottom right panel:* $f_{A\gamma}$ for the jetted outflow case from RSG progenitors. In this case, the breakout time is much longer. In this nonthermal photon regime, nuclei in high spin-down energy cases are readily photodisintegrated.

panel, the dashed black line denotes $f_{A\gamma} = 1$, a nucleus mass of $A = 56$ is assumed, and vertical gray shaded regions are marked for other relevant timescales. The lines inside the shaded regions show the results for each configuration considered in our B_{dip} and P_i space, while the boundaries of the shaded regions show the maxima and minima results across all cases. In the *top left panel*, we show the results for the spherical wind model. In Region A, $f_{A\gamma} < 1$ from the internal energy of the photons in that region. Although nuclei in Region A escape disintegration for $\lesssim 100$ s, the photons leaking into the region are able to disintegrate nuclei efficiently after this

point. Around t_{GJ} , nuclei are efficiently disintegrated, especially for high B_{dip} and low P_i protoneutron stars, but $f_{A\gamma} \sim 10$ around this time for the $B_{\text{dip}} = 10^{13}$ G and $P_i = 30$ ms case. In Region B, similarly, $f_{A\gamma} > 1$ only after $\gtrsim 100$ s, after which the nuclei can survive disintegration in the low B_{dip} /high P_i cases. These suggest that PNS with higher energy density - derived from their higher magnetorotational energy - are more efficient at disintegrating nuclei. The sharp rise in photodisintegration optical depth around ~ 100 s is because of the transition of photons from thermal to nonthermal spectra as well as a large increase in Γ_w occurring around the same

time.

B. Jetted outflow

In Region C, we consider the photons that are leaked from Region D: $U_{\gamma,C} = f_{\text{DC}}U_{\gamma,D}\Gamma_{\text{DC}}^2$, where $f_{\text{DC}} = \min(1/\tau_{T,D}, 1)$ is the leakage fraction from Region D to C and $\Gamma_{\text{DC}} = \Gamma_j\Gamma_{\text{cj}}(1 - \beta_j\beta_{\text{cj}})$ is the relative Lorentz factor between the pre-collimated jet and the collimated jet. The dynamical timescale is given by $t_{\text{exp},C} = R_{\text{cs}}/(\Gamma_j c)$. In Region D, $U_{\gamma,D} = 4\Gamma_{\text{DC}}^2 n_j m_p c^2$. This is valid for $\tau_{T,D} \gg 1$, and is realized for about $\sim 200 - 300$ s, so evaluation of results for the WR cases is reasonable (since $t_{\text{bo,WR}} \lesssim 200 - 300$ s), but should be noted in some BSG cases and the RSG case. Because the jet is collimated, the dynamical timescale is given by the advection timescale: $t_{\text{adv,D}} \sim R_h/(\Gamma_h c)$ (although, $\Gamma_h \sim 1$).

In the other three panels, we plot $f_{A\gamma}$ for WR, BSG, and RSG progenitors in the *top right*, *bottom left*, and *bottom right*, respectively. Although the values of $f_{A\gamma}$ do not change considerably depending on the progenitor, the breakout time, t_{bo} , changes dramatically between these systems. This has implications for nuclei survival, as nuclei can escape freely after the breakout time. Prior to $t_{\text{bo,WR}}$, $f_{A\gamma} \gg 1$ in Region D (and negligible in Region C) for high P_i cases, while $f_{A\gamma}$ decreases far below unity for low P_i cases. In this regime, photons are still thermal. For BSG progenitors, there is only one case where $f_{A\gamma} > 1$ before $t_{\text{bo,BSG}}$: $B_{\text{dip}} = 10^{15}$ G and $P_i = 10$ ms. In this one case, $f_{A\gamma}$ is only slightly larger than unity and occurs after t_{Th} , when photons are non-thermal. Although there are several cases in the figure where $f_{A\gamma} \gg 1$ after ~ 100 s in Regions C and D, this occurs in the scenarios with high PNS spindown energy. In such scenarios, the jets breakout very quickly, so nuclei are able to escape before this time. In the RSG case, $t_{\text{bo,RSG}} \gtrsim 300$ s is much later. Thus, nuclei can be exposed to nonthermal photons at late times and experience efficient photodisintegration. This disintegration occurs primarily for the high spindown energy cases (short P_i and higher B_{dip}). Note that these calculations are performed only up to 1000 s, however the breakout times of RSGs could be longer than this.

There are some similarities in the results between the spherical wind and jetted outflow scenarios. In general, it seems that at early times, when photons are thermal, the high spindown energy cases (with high B_{dip} and low P_i) are more efficiently photodisintegrated. However, the results at later times is more nuanced and depends on the details of nuclei escape in each model.

Based on these results, the distribution of the ambient photon field can have major consequences on the survivability of nuclei. Previous works generally found that nonthermal photon distributions result in photodisintegration timescales that are limited by the dynamical/expansion timescales of magnetized outflows. The photon distribution is not well known, which would affect

the outcome of nucleus survival. Synchrotron photons in the wind would be in the fast cooling regime [56, 57], while a broken power-law spectrum or the Band function can also be used in the jet [24, 44, 79]. The choice of minimum and maximum cutoff energies somewhat affects the energy at which $f_{A\gamma}$ decreases.

Because we determine new analytical approximations for the photodisintegration cross sections of heavy nuclei in Sec. II, we can estimate the efficiency of disintegration for heavy nuclei as well. This may be an important process to consider if outflows of supernovae produce heavy elements. In Fig. 5, we show how these results depend on mass number. In this figure, we only show the spherical wind model and WR jetted outflow models to show how efficiency scales with mass number. The results in black, for ‘Fe’ or iron are the same as the results in Fig. 4. We also show, in blue, orange, and purple, the results for selenium (‘Se’, $A = 79$), tellurium (‘Te’, $A = 128$), and platinum (‘Pt’, $A = 197$). As expected, $f_{A\gamma}$ increases monotonically with mass number, due to the mass dependence in the GDR cross section and because of the increased energy of the nuclei in the outflows, since they have energies of $\Gamma_x m_A c^2$.

V. DISCUSSION

Our study isolates the role of GDR photodisintegration for nuclei that are accelerated primarily by the bulk motion of the outflow, and it adopts a survival criterion ($f_{A\gamma} = 1$). Several important physical effects were not treated self-consistently and should be addressed in future work.

We assumed that nuclei are co-moving with the outflow and thus have characteristic energy $\Gamma_x m_A c^2$. However, the nuclei could be accelerated to even higher energies via internal shocks, shear, or magnetic reconnections (see, e.g., Ref. [44]). Higher-energy nuclei interact with different parts of the photon spectrum and may enter regimes where additional channels (e.g., photomeson production) become dominant. A self-consistent treatment coupling acceleration, radiation, and nuclear interactions is required to assess survival in such scenarios.

Using $f_{A\gamma} = 1$ as a binary survival criterion neglects intermediate regimes in which only a fraction of nuclei may disintegrate. For $0.1 \lesssim f_{A\gamma} \lesssim 1$, single interactions can create a mixed composition, while for $1 \lesssim f_{A\gamma} \lesssim 10$ repeated interactions can drive nuclei toward intermediate masses without complete destruction. Tracking the time-dependent mass and charge distribution (rather than a survival/no-survival outcome) is necessary to connect to observable UHECR composition, especially if candidate sources preferentially produce moderately heavy nuclei. We focused on the GDR channel, but at sufficiently high energies and/or in nonthermal photon fields, photomeson production and fragmentation can also become important [24, 80–82].

Spallation from nucleus–nucleus collisions can compete

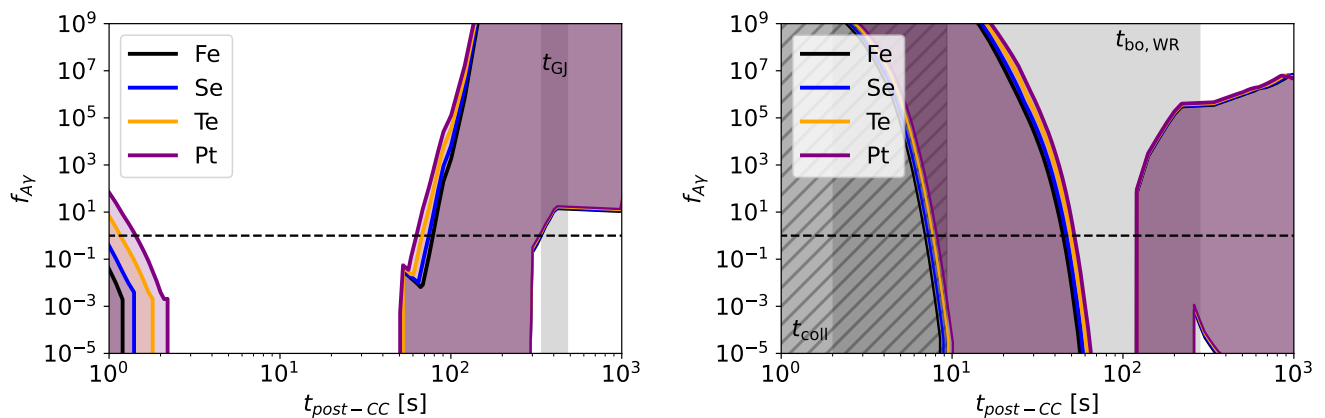


FIG. 5. Photodisintegration optical depths are shown as a function of time for our spherical wind model (*left panel*) and jetted outflow model (WR case, *right panel*), with varying nuclei composition. In black, we show the result for iron, which is the same result as the top row of Fig. 4, to compare with other cases. In blue, orange, and purple, we also show the efficiencies for selenium, tellurium, and platinum. This shows there is a slightly positive correlation of $f_{A\gamma}$ with mass number, and heavier nuclei are somewhat less likely to survive in general.

with photon-driven destruction when the baryon density is high and relative energies approach nuclear binding scales. Although we estimated that the spallation optical depth τ_{sp} can be comparable to $f_{A\gamma}$ for our benchmark models, we did not model spallation self-consistently. A detailed composition study should include both photodisintegration and spallation, and should assess implications for r -process nucleosynthesis and for the emergence of intermediate-mass nuclei (see also Refs. [43, 82, 83]).

If heavy nuclei are efficiently destroyed, the outflow becomes neutron rich and free neutrons may decouple dynamically from the charged component. Previous works have explored neutrino production from inelastic collisions of decoupled neutrons [56, 57], typically assuming proton-neutron-dominated composition. Our results suggest that this assumption may hold after ~ 100 s for spherical winds but can be strongly parameter dependent in jets, especially given the interplay among t_{Th} , the decoupling time, and t_{GJ} . A time-dependent model that tracks composition together with the radiation field and dynamical evolution is needed to make robust multi-messenger predictions.

VI. SUMMARY

Photodisintegration is one of the central concerns for modeling the sources of heavy nuclei. Candidate sources include GRBs, AGNs and TDEs, which are also considered as potential sources of heavy-nuclei UHECRs. In this work, based on TALYS simulations, we presented the updated GDR cross-section fits that are applicable to heavy nuclei up to $A = 197$.

We applied our formulae to magnetized outflows from protomagnetars, where the nuclei may be subject to bulk acceleration, and quantified photodisintegration efficien-

cies in a time-dependent manner. Across a broad range of central-engine parameters and progenitor structures, we found that nuclei survival is controlled by the competition between the escape timescale (set by t_{GJ} in spherical winds and by t_{bo} in jets) and the epoch of photon thermalization (modeled by t_{Th}), as well as by jet collimation effects that increase photon densities. These results delineate which combinations of engine parameters and progenitor envelopes can plausibly preserve heavy nuclei prior to their escape into the interstellar medium and constrain their contribution to the metal population within galaxies. They also provide a baseline for future, more complete treatments that couple particle acceleration, radiation, and full composition evolution. Furthermore, extending the present framework to different sources with their distinct radiation fields and dynamical timescales will be important for establishing whether sources of high-energy nuclei can preserve heavy or intermediate-mass composition up to the time of their escape.

ACKNOWLEDGMENTS

We thank Michael Unger and B. Theodore Zhang for useful discussions. This work was supported by NSF Grants Nos. AST-1908689 (K.M. and M.B.), AST-2108466 (K.M.), AST-2108467 (K.M.), AST-2308021 (K.M.), and PHY-2209420 (S.H.). We also acknowledge KAKENHI grant Nos. 20H01901 (K.M.), 20H05852 (K.M.), and 23H04899 (S.H.). M.B. acknowledges support from the Eberly Research Fellowship at the Pennsylvania State University and the Simons Collaboration on Extreme Electrodynamics of Compact Sources (SCEECs) Postdoctoral Fellowship at the Wisconsin Ice-Cube Particle Astrophysics Center (WIPAC), Univer-

sity of Wisconsin-Madison. This work was supported by World Premier International Research Center Initiative (WPI Initiative), MEXT, Japan.

DATA AVAILABILITY

The data are available from the authors upon reasonable request.

-
- [1] J. Blümer, R. Engel, and J. R. Hörandel, Cosmic rays from the knee to the highest energies, *Progress in Particle and Nuclear Physics* **63**, 293 (2009).
- [2] K. Kotera and A. V. Olinto, The astrophysics of ultrahigh-energy cosmic rays, *Annual Review of Astronomy and Astrophysics* **49**, 119 (2011).
- [3] R. Alves Batista, J. Biteau, M. Bustamante, K. Dolag, R. Engel, K. Fang, K.-H. Kampert, D. Kostunin, M. Mostafa, K. Murase, and et al., Open questions in cosmic-ray research at ultrahigh energies, *Frontiers in Astronomy and Space Sciences* **6**, 23 (2019).
- [4] L. A. Anchordoqui, Ultra-high-energy cosmic rays, *Physics Reports* **801**, 1 (2019).
- [5] A. Aab *et al.* (Pierre Auger), The Pierre Auger Cosmic Ray Observatory, *Nucl. Instrum. Meth. A* **798**, 172 (2015), [arXiv:1502.01323 \[astro-ph.IM\]](#).
- [6] T. Abu-Zayyad, R. Aida, M. Allen, R. Anderson, R. Azuma, E. Barcikowski, J. W. Belz, D. R. Bergman, S. A. Blake, R. Cady, and et al., The cosmic-ray energy spectrum observed with the surface detector of the telescope array experiment, *The Astrophysical Journal* **768**, L1 (2013).
- [7] K. Greisen, End to the cosmic ray spectrum?, *Phys. Rev. Lett.* **16**, 748 (1966).
- [8] G. T. Zatsepin and V. A. Kuz'min, Upper Limit of the Spectrum of Cosmic Rays, *Soviet Journal of Experimental and Theoretical Physics Letters* **4**, 78 (1966).
- [9] J. Abraham *et al.* (Pierre Auger), Observation of the suppression of the flux of cosmic rays above 4×10^{19} eV, *Phys. Rev. Lett.* **101**, 061101 (2008), [arXiv:0806.4302 \[astro-ph\]](#).
- [10] R. U. Abbasi, T. Abu-Zayyad, M. Allen, J. F. Amman, G. Archbold, K. Belov, J. W. Belz, S. Y. Ben Zvi, D. R. Bergman, S. A. Blake, O. A. Brusova, G. W. Burt, C. Cannon, Z. Cao, B. C. Connolly, W. Deng, Y. Fedorova, C. B. Finley, R. C. Gray, W. F. Hanlon, C. M. Hoffman, M. H. Holzschneider, G. Hughes, P. Hüntemeyer, B. F. Jones, C. C. H. Jui, K. Kim, M. A. Kirn, E. C. Loh, M. M. Maestas, N. Manago, L. J. Marek, K. Martens, J. A. J. Matthews, J. N. Matthews, S. A. Moore, A. O'Neill, C. A. Painter, L. Perera, K. Reil, R. Riehle, M. Roberts, D. Rodriguez, N. Sasaki, S. R. Schnetzer, L. M. Scott, G. Sinijs, J. D. Smith, P. Sokolsky, C. Song, R. W. Springer, B. T. Stokes, S. B. Thomas, J. R. Thomas, G. B. Thomson, D. Tupa, S. Westerhoff, L. R. Wiencke, X. Zhang, and A. Zech (High Resolution Fly's Eye Collaboration), First observation of the greisen-zatsepin-kuzmin suppression, *Phys. Rev. Lett.* **100**, 101101 (2008).
- [11] A. A. Halim *et al.* (Pierre Auger), Constraining the sources of ultra-high-energy cosmic rays across and above the ankle with the spectrum and composition data measured at the Pierre Auger Observatory, *JCAP* **05**, 024, [arXiv:2211.02857 \[astro-ph.HE\]](#).
- [12] L. A. Anchordoqui, M. T. Dova, T. P. McCauley, S. Reucroft, and J. D. Swain, Possible explanation for the tail of the cosmic ray spectrum, *Phys. Lett. B* **482**, 343 (2000), [arXiv:astro-ph/9912081](#).
- [13] B. T. Zhang, K. Murase, N. Ekanger, M. Bhattacharya, and S. Horiuchi, Ultraheavy Ultrahigh-Energy Cosmic Rays (2024), [arXiv:2405.17409 \[astro-ph.HE\]](#).
- [14] Y. Jiang, B. T. Zhang, and K. Murase, Energetics of ultrahigh-energy cosmic-ray nuclei, *Phys. Rev. D* **104**, 043017 (2021).
- [15] M. Kuznetsov and P. Tinyakov, Uhecr mass composition at highest energies from anisotropy of their arrival directions, *Journal of Cosmology and Astroparticle Physics* **2021** (04), 065.
- [16] C. A. Norman, D. B. Melrose, and A. Achterberg, The origin of cosmic rays above 10 18.5 ev, *The Astrophysical Journal* **454**, 60 (1995).
- [17] C. D. Dermer, S. Razzaque, J. D. Finke, and A. Atoyan, Ultra-high-energy cosmic rays from black hole jets of radio galaxies, *New J. Phys.* **11**, 065016 (2009).
- [18] A. Pe'er, K. Murase, and P. Meszaros, Radio Quiet AGNs as Possible Sources of Ultra-high Energy Cosmic Rays, *Phys. Rev. D* **80**, 123018 (2009), [arXiv:0911.1776 \[astro-ph.HE\]](#).
- [19] H. Takami and S. Horiuchi, The production of ultra high energy cosmic rays during the early epochs of radio-loud agn, *Astroparticle Physics* **34**, 749 (2011).
- [20] K. Murase, C. D. Dermer, H. Takami, and G. Migliori, Blazars as Ultra-High-Energy Cosmic-Ray Sources: Implications for TeV Gamma-Ray Observations, *Astrophys. J.* **749**, 63 (2012), [arXiv:1107.5576 \[astro-ph.HE\]](#).
- [21] E. Waxman, Cosmological gamma-ray bursts and the highest energy cosmic rays, *Phys. Rev. Lett.* **75**, 386 (1995).
- [22] M. Milgrom and V. Usov, Ascertaining the core collapse supernova mechanism: The state of the art and the road ahead, *ApJL* **449**, L37 (1995).
- [23] K. Murase, K. Ioka, S. Nagataki, and T. Nakamura, High Energy Neutrinos and Cosmic-Rays from Low-Luminosity Gamma-Ray Bursts?, *Astrophys. J. Lett.* **651**, L5 (2006), [arXiv:astro-ph/0607104](#).
- [24] K. Murase, K. Ioka, S. Nagataki, and T. Nakamura, High-energy cosmic-ray nuclei from high- and low-luminosity gamma-ray bursts and implications for multi-messenger astronomy, *Phys. Rev. D* **78**, 023005 (2008),

- arXiv:0801.2861 [astro-ph].
- [25] R.-Y. Liu and X.-Y. Wang, Energy spectrum and chemical composition of ultrahigh energy cosmic rays from semi-relativistic hypernovae, *Astrophys. J.* **746**, 40 (2012), arXiv:1111.6256 [astro-ph.HE].
- [26] J. Arons, Magnetars in the metagalaxy: An origin for ultra-high-energy cosmic rays in the nearby universe, *The Astrophysical Journal* **589**, 871 (2003).
- [27] K. Murase, P. Meszaros, and B. Zhang, Probing the birth of fast rotating magnetars through high-energy neutrinos, *Phys. Rev. D* **79**, 103001 (2009).
- [28] K. Fang, K. Kotera, and A. V. Olinto, Newly-born pulsars as sources of ultrahigh energy cosmic rays, *Astrophys. J.* **750**, 118 (2012), arXiv:1201.5197 [astro-ph.HE].
- [29] K. Fang, K. Kotera, K. Murase, and A. V. Olinto, Testing the Newborn Pulsar Origin of Ultrahigh Energy Cosmic Rays with EeV Neutrinos, *Phys. Rev. D* **90**, 103005 (2014), [Erratum: Phys.Rev.D 92, 129901 (2015)], arXiv:1311.2044 [astro-ph.HE].
- [30] H. Takami, K. Kyutoku, and K. Ioka, High-Energy Radiation from Remnants of Neutron Star Binary Mergers, *Phys. Rev. D* **89**, 063006 (2014), arXiv:1307.6805 [astro-ph.HE].
- [31] X. Rodrigues, D. Biehl, D. Boncioli, and A. M. Taylor, Binary neutron star merger remnants as sources of cosmic rays below the “Ankle”, *Astropart. Phys.* **106**, 10 (2019), arXiv:1806.01624 [astro-ph.HE].
- [32] K. Murase and M. Fukugita, Energetics of High-Energy Cosmic Radiations, *Phys. Rev. D* **99**, 063012 (2019), arXiv:1806.04194 [astro-ph.HE].
- [33] G. R. Farrar, Binary Neutron Star Mergers as the Source of the Highest Energy Cosmic Rays, *Phys. Rev. Lett.* **134**, 081003 (2025), arXiv:2405.12004 [astro-ph.HE].
- [34] D. Caprioli, “Espresso” Acceleration of Ultra-high-energy Cosmic Rays, *Astrophys. J. Lett.* **811**, L38 (2015), arXiv:1505.06739 [astro-ph.HE].
- [35] S. S. Kimura, K. Murase, and B. T. Zhang, Ultrahigh-energy Cosmic-ray Nuclei from Black Hole Jets: Recycling Galactic Cosmic Rays through Shear Acceleration, *Phys. Rev. D* **97**, 023026 (2018), arXiv:1705.05027 [astro-ph.HE].
- [36] R. Mbarek and D. Caprioli, Bottom-up Acceleration of Ultra-High-Energy Cosmic Rays in the Jets of Active Galactic Nuclei, *Astrophys. J.* **886**, 8 (2019), arXiv:1904.02720 [astro-ph.HE].
- [37] R. Mbarek, D. Caprioli, and K. Murase, High-energy Neutrino Emission from Espresso-reaccelerated Ions in Jets of Active Galactic Nuclei, *Astrophys. J.* **942**, 37 (2023), arXiv:2207.07130 [astro-ph.HE].
- [38] B. T. Zhang, K. Murase, S. S. Kimura, S. Horiuchi, and P. Mészáros, Low-luminosity gamma-ray bursts as the sources of ultrahigh-energy cosmic ray nuclei, *Phys. Rev. D* **97**, 083010 (2018), arXiv:1712.09984 [astro-ph.HE].
- [39] D. Boncioli, D. Biehl, and W. Winter, On the common origin of cosmic rays across the ankle and diffuse neutrinos at the highest energies from low-luminosity Gamma-Ray Bursts, *Astrophys. J.* **872**, 110 (2019), arXiv:1808.07481 [astro-ph.HE].
- [40] B. T. Zhang and K. Murase, Ultrahigh-energy cosmic-ray nuclei and neutrinos from engine-driven supernovae, *Phys. Rev. D* **100**, 103004 (2019), arXiv:1812.10289 [astro-ph.HE].
- [41] B. T. Zhang, K. Murase, F. Oikonomou, and Z. Li, High-energy cosmic ray nuclei from tidal disruption events: Origin, survival, and implications, *Phys. Rev. D* **96**, 063007 (2017), [Addendum: Phys.Rev.D 96, 069902 (2017)], arXiv:1706.00391 [astro-ph.HE].
- [42] B. D. Metzger, D. Giannios, and S. Horiuchi, Heavy nuclei synthesized in gamma-ray burst outflows as the source of ultrahigh energy cosmic rays, *Monthly Notices of the Royal Astronomical Society* **415**, 2495 (2011).
- [43] S. Horiuchi, K. Murase, K. Ioka, and P. Mészáros, The survival of nuclei in jets associated with core-collapse supernovae and gamma-ray bursts, *The Astrophysical Journal* **753**, 69 (2012).
- [44] M. Bhattacharya, S. Horiuchi, and K. Murase, On the synthesis of heavy nuclei in protomagnetar outflows and implications for ultra-high energy cosmic rays, *Mon. Not. Roy. Astron. Soc.* **514**, 6011 (2022), arXiv:2111.05863 [astro-ph.HE].
- [45] N. Ekanger, M. Bhattacharya, and S. Horiuchi, Systematic exploration of heavy element nucleosynthesis in protomagnetar outflows, *Mon. Not. Roy. Astron. Soc.* **513**, 405 (2022), arXiv:2201.03576 [astro-ph.HE].
- [46] N. Ekanger, M. Bhattacharya, and S. Horiuchi, Nucleosynthesis in outflows of compact objects and detection prospects of associated kilonovae, *Mon. Not. Roy. Astron. Soc.* **525**, 2040 (2023), arXiv:2303.00765 [astro-ph.HE].
- [47] T. A. Thompson, P. Chang, and E. Quataert, Magnetar spin-down, hyperenergetic supernovae, and gamma-ray bursts, *The Astrophysical Journal* **611**, 380 (2004).
- [48] X.-Y. Wang, S. Razzaque, and P. Meszaros, On the Origin and Survival of UHE Cosmic-Ray Nuclei in GRBs and Hypernovae, *Astrophys. J.* **677**, 432 (2008), arXiv:0711.2065 [astro-ph].
- [49] J. L. Puget, F. W. Stecker, and J. H. Bredekamp, Photonuclear interactions of ultrahigh energy cosmic rays and their astrophysical consequences., *ApJ* **205**, 638 (1976).
- [50] F. W. Stecker and M. H. Salamon, Photodisintegration of ultrahigh-energy cosmic rays: A New determination, *Astrophys. J.* **512**, 521 (1999), arXiv:astro-ph/9808110.
- [51] E. Khan, S. Goriely, D. Allard, E. Parizot, T. Suomijarvi, A. J. Koning, S. Hilaire, and M. C. Duijvestijn, Photodisintegration of ultra-high-energy cosmic rays revisited, *Astropart. Phys.* **23**, 191 (2005), arXiv:astro-ph/0412109.
- [52] M. Bhattacharya, J. A. Carpio, K. Murase, and S. Horiuchi, High-energy neutrino emission from magnetised jets of rapidly rotating protomagnetars, *Mon. Not. Roy. Astron. Soc.* **521**, 2391 (2023), arXiv:2210.08029 [astro-ph.HE].
- [53] A. M. Soderberg, S. R. Kulkarni, E. Nakar, E. Berger, P. B. Cameron, D. B. Fox, D. Frail, A. Gal-Yam, R. Sari, S. B. Cenko, M. Kasliwal, R. A. Chevalier, T. Piran, P. A. Price, B. P. Schmidt, G. Pooley, D. S. Moon, B. E. Penprase, E. Ofek, A. Rau, N. Gehrels, J. A. Nousek, D. N. Burrows, S. E. Persson, and P. J. McCarthy, Relativistic ejecta from X-ray flash XRF 060218 and the rate of cosmic explosions, *Nature* **442**, 1014 (2006), arXiv:astro-ph/0604389 [astro-ph].
- [54] R. Margutti, A. M. Soderberg, M. H. Wieringa, P. G. Edwards, R. A. Chevalier, B. J. Morsony, R. Barniol Duran, L. Sironi, B. A. Zauderer, D. Milisavljevic, A. Kamble, and E. Pian, The Signature of the Central Engine in the Weakest Relativistic Explosions: GRB 100316D, *ApJ* **778**, 18 (2013), arXiv:1308.1687 [astro-ph.HE].
- [55] R. Margutti, D. Milisavljevic, A. M. Soderberg, C. Guidorzi, B. J. Morsony, N. Sanders, S. Chakraborti,

- A. Ray, A. Kamble, M. Drout, J. Parrent, A. Zauderer, and L. Chomiuk, Relativistic Supernovae have Shorter-lived Central Engines or More Extended Progenitors: The Case of SN 2012ap, *ApJ* **797**, 107 (2014), [arXiv:1402.6344 \[astro-ph.HE\]](#).
- [56] K. Murase, B. Dasgupta, and T. A. Thompson, Quasithermal Neutrinos from Rotating Protoneutron Stars Born during Core Collapse of Massive Stars, *Phys. Rev. D* **89**, 043012 (2014), [arXiv:1303.2612 \[astro-ph.HE\]](#).
- [57] J. A. Carpio, N. Ekanger, M. Bhattacharya, K. Murase, and S. Horiuchi, Quasithermal GeV neutrinos from neutron-loaded magnetized outflows in core-collapse supernovae: Spectra and light curves, *Phys. Rev. D* **110**, 083012 (2024), [arXiv:2310.16823 \[astro-ph.HE\]](#).
- [58] K. Murase and J. F. Beacom, Neutrino background flux from sources of ultrahigh-energy cosmic-ray nuclei, *Phys. Rev. D* **81**, 123001 (2010), [arXiv:1003.4959 \[astro-ph.HE\]](#).
- [59] K. Murase and J. F. Beacom, Very-High-Energy Gamma-Ray Signal from Nuclear Photodisintegration as a Probe of Extragalactic Sources of Ultrahigh-Energy Nuclei, *Phys. Rev. D* **82**, 043008 (2010), [arXiv:1002.3980 \[astro-ph.HE\]](#).
- [60] B. T. Zhang and K. Murase, Nuclear and electromagnetic cascades induced by ultra-high-energy cosmic rays in radio galaxies: implications for Centaurus A, *Mon. Not. Roy. Astron. Soc.* **524**, 76 (2023), [arXiv:2302.14048 \[astro-ph.HE\]](#).
- [61] S. Karakula and W. Tkaczyk, The formation of the cosmic ray energy spectrum by a photon field, *Astroparticle Physics* **1**, 229 (1993).
- [62] A. J. Koning and D. Rochman, Modern Nuclear Data Evaluation with the TALYS Code System, *Nuclear Data Sheets* **113**, 2841 (2012).
- [63] A. J. Koning, D. Rochman, J. C. Sublet, N. Dzysiuk, M. Fleming, and S. van der Marck, TENDL: Complete Nuclear Data Library for Innovative Nuclear Science and Technology, *Nuclear Data Sheets* **155**, 1 (2019).
- [64] R. B. Firestone, The Origin of the Giant Dipole Resonance (2020), [arXiv:2009.03356 \[nucl-th\]](#).
- [65] M. Goldhaber and E. Teller, On nuclear dipole vibrations, *Phys. Rev.* **74**, 1046 (1948).
- [66] S. Agostinelli *et al.* (GEANT4), GEANT4—a simulation toolkit, *Nucl. Instrum. Meth. A* **506**, 250 (2003).
- [67] J. P. Rachen, *Interaction Processes and Statistical Properties of the Propagation of Cosmic Rays in Photon Backgrounds*, Ph.D. thesis, Max-Planck-Institute for Radioastronomy, Bonn (1996).
- [68] D. Allard, E. Parizot, E. Khan, S. Goriely, and A. V. Olinto, UHE nuclei propagation and the interpretation of the ankle in the cosmic-ray spectrum, *Astron. Astrophys.* **443**, L29 (2005), [arXiv:astro-ph/0505566](#).
- [69] P. Goldreich and W. H. Julian, Pulsar Electrodynamics, *ApJ* **157**, 869 (1969).
- [70] N. Bucciantini, J. Arons, and E. Amato, Modelling spectral evolution of pulsar wind nebulae inside supernova remnants, *MNRAS* **410**, 381 (2011), [arXiv:1005.1831 \[astro-ph.HE\]](#).
- [71] A. N. Timokhin and A. K. Harding, On the polar cap cascade pair multiplicity of young pulsars, *Astrophys. J.* **810**, 144 (2015), [arXiv:1504.02194 \[astro-ph.HE\]](#).
- [72] K. Murase, K. Kashiyama, K. Kiuchi, and I. Bartos, Gamma-Ray and Hard X-Ray Emission from Pulsar-Aided Supernovae as a Probe of Particle Acceleration in Embryonic Pulsar Wind Nebulae, *Astrophys. J.* **805**, 82 (2015), [arXiv:1411.0619 \[astro-ph.HE\]](#).
- [73] K. Kashiyama, K. Murase, I. Bartos, K. Kiuchi, and R. Margutti, Multi-messenger Tests for Fast-spinning Newborn Pulsars Embedded in Stripped-envelope Supernovae, *ApJ* **818**, 94 (2016), [arXiv:1508.04393 \[astro-ph.HE\]](#).
- [74] B. D. Metzger, D. Giannios, T. A. Thompson, N. Bucciantini, and E. Quataert, The protomagnetar model for gamma-ray bursts, *Monthly Notices of the Royal Astronomical Society* **413**, 2031 (2011).
- [75] J. A. Pons, S. Reddy, M. Prakash, J. M. Lattimer, and J. A. Miralles, Evolution of proto-neutron stars, *The Astrophysical Journal* **513**, 780 (1999).
- [76] G. Drenkhahn, Acceleration of GRB outflows by Poynting flux dissipation, *A&A* **387**, 714 (2002), [arXiv:astro-ph/0112509 \[astro-ph\]](#).
- [77] O. Bromberg, J. Granot, and T. Piran, On the composition of GRBs' Collapsar jets, *Mon. Not. Roy. Astron. Soc.* **450**, 1077 (2015), [arXiv:1407.0123 \[astro-ph.HE\]](#).
- [78] K. Murase, M. Mukhopadhyay, A. Kheirandish, S. S. Kimura, and K. Fang, Neutrinos from the Brightest Gamma-Ray Burst?, *Astrophys. J. Lett.* **941**, L10 (2022), [arXiv:2210.15625 \[astro-ph.HE\]](#).
- [79] D. Giannios and H. C. Spruit, Spectral and timing properties of a dissipative GRB photosphere, *Astron. Astrophys.* **469**, 1 (2007), [arXiv:astro-ph/0611385](#).
- [80] N. Globus, D. Allard, R. Mochkovitch, and E. Parizot, UHECR acceleration at GRB internal shocks, *Mon. Not. Roy. Astron. Soc.* **451**, 751 (2015), [arXiv:1409.1271 \[astro-ph.HE\]](#).
- [81] D. Boncioli, A. Fedynitch, and W. Winter, Nuclear Physics Meets the Sources of the Ultra-High Energy Cosmic Rays, *Sci. Rep.* **7**, 4882 (2017), [arXiv:1607.07989 \[astro-ph.HE\]](#).
- [82] L. Morejon, A. Fedynitch, D. Boncioli, D. Biehl, and W. Winter, Improved photomeson model for interactions of cosmic ray nuclei, *JCAP* **11**, 007, [arXiv:1904.07999 \[astro-ph.HE\]](#).
- [83] J. C. David, Spallation reactions: A successful interplay between modeling and applications, *Eur. Phys. J. A* **51**, 68 (2015), [arXiv:1505.03282 \[nucl-ex\]](#).